

Boise State University

ScholarWorks

Geosciences Faculty Publications and
Presentations

Department of Geosciences

12-28-2023

Exploring Background Noise with a Large-N Infrasonic Array: Waterfalls, Thunderstorms, and Earthquakes

L. T. Scamfer

Boise State University

J. F. Anderson

Boise State University

—



Geophysical Research Letters®



RESEARCH LETTER

10.1029/2023GL104635

Exploring Background Noise With a Large-N Infrasound Array: Waterfalls, Thunderstorms, and Earthquakes

L. T. Scamfer¹  and J. F. Anderson¹ 

¹Department of Geosciences, Boise State University, Boise, ID, USA

Key Points:

- A 22-element infrasound array is used to identify weak acoustic sources that could otherwise be hidden in background noise
- Infrasound from thunderstorms, earthquakes, and both local and distant waterfalls is observed
- Large-N infrasound monitoring enables detection of distant waterfall infrasound, with potential applications in hydrologic monitoring

Supporting Information:

Supporting Information may be found in the online version of this article.

Correspondence to:

L. T. Scamfer,
loganscamfer@gmail.com

Citation:

Scamfer, L. T., & Anderson, J. F. (2023). Exploring background noise with a large-N infrasound array: Waterfalls, thunderstorms, and earthquakes. *Geophysical Research Letters*, 50, e2023GL104635. <https://doi.org/10.1029/2023GL104635>

Received 28 MAY 2023

Accepted 30 NOV 2023

Abstract Ambient infrasound noise contains an abundance of information that is typically overlooked due to limitations of typical infrasound arrays. To evaluate the ability of large-N infrasound arrays to identify weak signals hidden in background noise, we examine data from a 22-element array in central Idaho, USA, spanning 58 days using a standard beamforming method. Our results include nearly continuous detections of diverse weak signals from infrasonic radiators, sometimes at surprising distances. We observe infrasound from both local (8 km) and distant (195 km) waterfalls. Thunderstorms and earthquakes are also notable sources, with distant thunderstorm infrasound observed from ~800 to 900 km away. Our findings show that large-N infrasound arrays can detect very weak signals below instrument and environmental noise floors, including from multiple simultaneous sources, enabling new infrasound monitoring applications and helping map the composition of background noise wavefields.

Plain Language Summary Infrasound, or sound with a frequency below what humans can generally hear, is often produced by various earth processes. Compared to audible sound, infrasound can travel longer distances while retaining more energy, making it especially useful for remote monitoring purposes. Infrasound arrays are stations that consist of multiple infrasonic microphones, which use time-delays between sensors to determine the direction of a wave's arrival. Using a greater number of microphones allows for the improved detection of weak signals, a technique referred to as "large-N." Our study uses an arrangement of 22 microphones to locate sources of infrasound, such as waterfalls, thunderstorms, and earthquakes. Infrasound from waterfalls was identified at both nearby and distant locations, reaching almost 200 km. Thunderstorms and earthquakes were also recorded, with thunder infrasound coming from distances of nearly 900 km. Our results show that large-N infrasound can reveal earth processes that may otherwise go unnoticed.

1. Introduction

Infrasound is a widely used geophysical tool to remotely monitor earth processes and atmospheric properties. Major applications of infrasound include the study of volcanoes (Fee & Matoza, 2013; Johnson & Ripepe, 2011), anthropogenic explosions (Arrowsmith et al., 2008; Che et al., 2014), earthquakes (Johnson et al., 2020; Mutschlechner, 2005), and thunderstorms (Anderson et al., 2014; Farges et al., 2021). Other infrasound applications have expanded to investigate flow processes, including avalanches (Johnson et al., 2021; Ulivieri et al., 2011), debris flows (Kogelnig et al., 2014), river rapids (Ronan et al., 2017; Tatum et al., 2023), waterfalls (Johnson et al., 2006) and lahars (Bosa et al., 2021; Sanderson et al., 2021).

Traditional infrasound arrays (using three or more sensors) are effective at locating the direction of acoustic sources when one source is dominant, but large-N arrays (using many more than the minimum 3 sensors to estimate slowness vectors) are a strategy to more effectively detect weak signals that may otherwise be hidden in background noise, or obscured by a more dominant source (Evers & Haak, 2005). The benefits of large-N infrasound arrays are not only limited to the detection of weak signals, but also the ability to resolve source directions and slowness values with significantly finer detail (Anderson et al., 2023).

These advantages of large-N arrays suggest they may help glean source information from low-amplitude background noise that is normally discarded due to its low signal-to-noise ratio, raising our research question of what can be learned about infrasound sources by studying background noise with a large-N array. Using our two month data set recorded on a 22-sensor array in a low noise setting, we demonstrate the capability of a large-N infrasound array to resolve low-level background noise from diverse, weak infrasonic sources. We identify waterfall, thunder, and low-magnitude earthquake infrasound; these sources often occur simultaneously and can be detected (in different time windows) independently. Our findings include the first example of stratosphere-refracted waterfall

© 2023. The Authors.

This is an open access article under the terms of the [Creative Commons Attribution License](https://creativecommons.org/licenses/by/4.0/), which permits use, distribution and reproduction in any medium, provided the original work is properly cited.

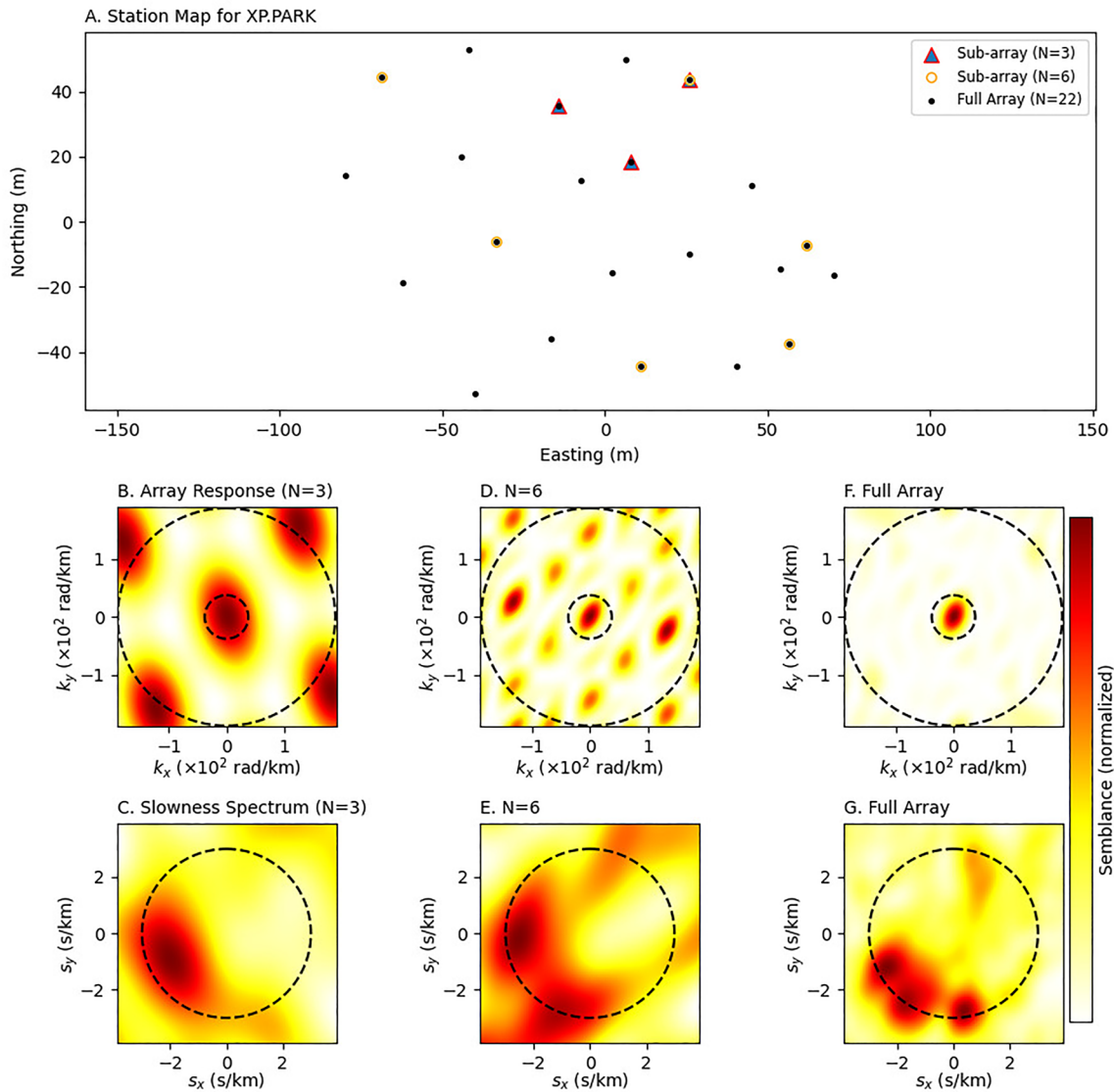


Figure 1. (a) Map of the full PARK array and, for comparison, a three-element and six-element sub-array representative of common infrasound arrays. (b and c) The array response and slowness spectrum of the three-element sub-array. The array response contains a wide main lobe around the origin, as well as significant nearby sidelobes. A period of data beamformed by the sub-array produces the slowness spectrum in panel (c), identified as a single source. (d and e) The array response and slowness spectrum of the six-element sub-array. Although the blurring effect in the slowness spectrum for both the 3 and 6-element arrays is significant, it can be improved by deconvolving their respective array response functions, for example, by Lucy-Richardson (Nishida et al., 2008), or CLEAN (Anderson et al., 2023). (f and g) The array response and slowness spectrum of the full array. The array response of the full array lacks the deficiencies of the previous sub-arrays. In the slowness spectrum, the region in the southwest identified as a single source by the sub-array (c) is revealed by the full array to be in fact three distinct sources. Modified from Anderson et al. (2023).

infrasound at a distance of ~ 195 km, and an uncommonly distant detection of thunder infrasound 800–900 km away.

2. Methods

The PARK station is a 22-element infrasound array (Figure 1a) located in the mountains of central Idaho, USA, which was established following the 2020 M6.5 Stanley, Idaho Earthquake to monitor aftershock activity. Each sensor in the array was a Gem infrasound logger (Anderson et al., 2018) with a flat response between 0.039 and 27 Hz and a root-mean-square self-noise of 2.75 mPa in the 5–20 Hz band of interest. As a “node”-style instrument (small size, internal batteries, cable-free) the Gem reduced the normal challenges associated with remote

arrays of this size via its ease of deployment, concealment, and infrequent need for battery replacements. The station began monitoring on 15 April 2020 and continued through 11 June 2020.

Compared to a 3 or 6-element array, arrays with more elements provide superior source discrimination/slowness resolution, and redundancy (Figures 1c, 1e, and 1g, Figure S5 in Supporting Information S1). Large spacing between the most distant sensors results in superior array resolution (more compact main lobe in array response), whereas short spacing between the nearest sensors reduces susceptibility to spatial aliasing and helps ensure good signal coherence among sensors. Using more sensors makes it possible to accomplish both objectives at once. In this paper, we define “large-N” as the use of many more sensors than the minimum required for locating a source's position or direction with the objective of improved resolution of source characteristics, and we consider our array of 22 elements to be a large-N array. The array was placed in a wooded area to help reduce wind noise, and individual elements were spread over an area of ~ 100 by 150 m (Figure 1a). Topographic obstructions from surrounding mountains are present, but minimal. Obstruction angles range from ~ 1 to 4° from horizontal.

Back-azimuths and horizontal slownesses are found via a slowness vector grid search using the `array_processing()` function in the Python package `ObsPy` (Krischer et al., 2015). X and Y slowness grid values range from -4 to 4 s/km, with 0.1 s/km spacing. Array processing used 10-s sliding windows with 50% overlap. Low and high frequency parameters (the minimum and maximum frequencies that are used in frequency domain beamforming) were 5 and 20 Hz respectively. We define the beamformed result of a single time window as a “detection.” For color-mapped panels in Figure 2, we assigned backazimuth values to 2.5° bins, and horizontal slowness to 0.2 s/km bins.

3. Results and Discussion

During the 58-day study period, infrasound data from PARK station was analyzed to identify different processes captured by the array. Although the primary goal of establishing this array was to monitor aftershocks, many additional infrasonic radiators were detected by PARK. Waterfalls, thunderstorms, and earthquakes are all identified as significant sources of infrasound in this region (Figure 2).

3.1. Local Infrasound From a Small Waterfall

Waterfalls and other whitewater features are significant sources of infrasound. We identify two radiators of waterfall infrasound captured by the PARK array: Lady Face Falls (LFF), and a combination of Twin and Shoshone Falls.

LFF is located 7.88 km from PARK on Stanley Lake Creek, a perennial mountain stream whose spring and summer flow is primarily reliant on melting snowpack (Figure 3a). LFF is a small waterfall, with an approximate total height of several meters.

The infrasound signal attributed to LFF is quiet and continuous, although sometimes undetected when wind noise is significant. Both slowness and backazimuth are more constrained during the pure waterfall signal and later spread out—a relationship seen on all days—most likely due to wind noise (Figures 2c and 2d). The signal is not present until the last day of April, and then becomes the dominant source of sound received by PARK (Figure 2a). While this waterfall signal is present in the 5–20 Hz band of interest, it is completely absent below 2 Hz, and intermittent in the 2–5 Hz band (Figures S1–S3 in Supporting Information S1); this corresponds well to the spectrum of infrasound recorded near the waterfall having little energy below 2 Hz (Figure S4 in Supporting Information S1) and to the fact that ambient infrasound noise increases in power spectral density at lower frequencies. Although the Boise metropolitan area lies along a similar backazimuth as LFF at a range of ~ 125 km, we find an anthropogenic source unlikely given its distance and dependence on upper atmospheric conditions for refraction, and the lack of human temporal patterns. On the other hand, infrasound originating from 232° backazimuth has characteristics that are well-defined by a waterfall source. The detectability of the falls is affected by wind noise and streamflow, which both vary daily and on longer timescales.

We attribute the beginning of the waterfall signal to rising temperatures, initiating considerable melt in the snowmelt-dominated Stanley Lake basin (Figure 3) and increasing discharge at LFF. Partial snow cover of the waterfall early in the season (which we did observe in an early-spring site visit) may also muffle infrasound at its source (Capelli et al., 2016), so the loss of the waterfall's snow cover may also explain the signal's onset. Stanley

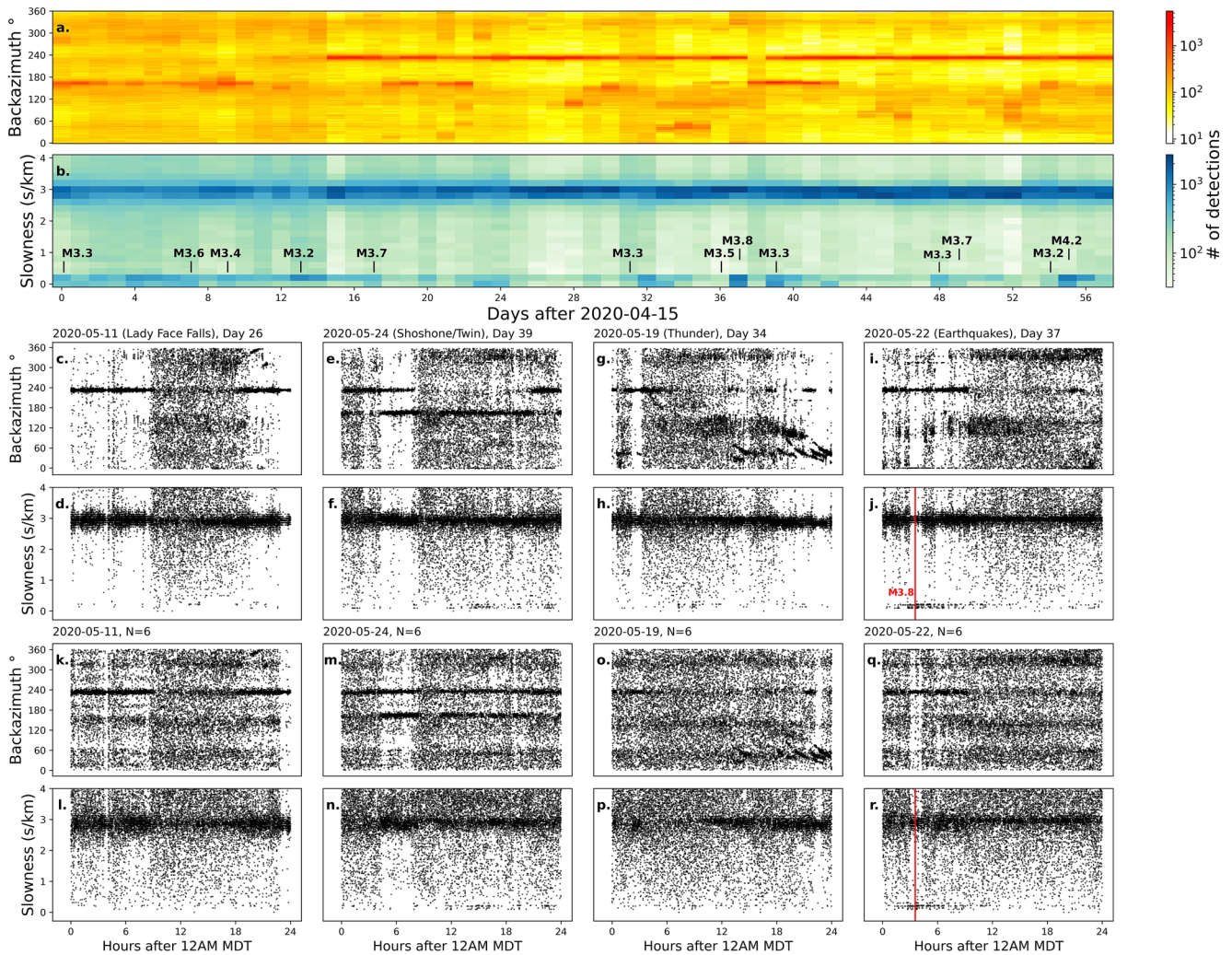


Figure 2. Overview of infrasound detection characteristics at PARK station from 15 April 2020 to 11 June 2020. (a) Backazimuth versus time, colors indicate the number of detections each day in 2.5° bins. Two backazimuths with especially high detections correspond to waterfalls: Lady Face Falls (LFF) ($\sim 232^\circ$, 7.9 km distance) and Twin/Shoshone Falls ($\sim 165^\circ$, which, at ~ 195 km, cannot be distinguished). (b) Horizontal slowness versus time. Days with a higher density of detections with near-zero slowness are indicative of seismic activity (Day 37, panels (i) and (j)). (c and d) On 11 May 2020 the first 8 hrs show nearly every detection centered about $\sim 232^\circ$, the direction of LFF. (e and f) On 24 May 2020, the band of detections at $\sim 165^\circ$ backazimuth are inferred to be radiated from Shoshone and Twin Falls, almost 200 km away. (g and h) On 19 May 2020 repeated, slowly-changing backazimuth detections are identified as thunderstorms (see Figure 5). (i and j) On 22 May 2020 the cluster of detections with near-zero slowness is identified as primary earthquake infrasound. (k–r) A recreation of panels c–j with a subarray of $N = 6$ elements.

Lake Creek is ungauged, so we are unable to directly correlate discharge with infrasound characteristics in the 2020 data set. However, in follow-up visits in 2023, we estimated its discharge on the order of ~ 0.25 m^3/s (22 April 2023, early in the melt-off) to ~ 4 m^3/s (20 May 2023, in the middle of the spring melt-off). During this follow-up study period, infrasound power measured ~ 35 m from the waterfall during periods of low background noise show amplitude lowest at the beginning and highest at the end of the recording period, corroborating the seasonal rise in waterfall infrasound detected remotely in our 2020 large- N data set (Figure S4 in Supporting Information S1). Given the small size of LFF and its distance from PARK, the amount of detectable infrasound highlights the utility of large- N arrays with weak sources.

3.2. Distant Infrasound From Large Waterfalls

Located on the Snake River ~ 195 km from PARK at a backazimuth of $\sim 164.5^\circ$, Twin Falls and Shoshone Falls are among the largest waterfalls in the region (dropping 60 and 65 m respectively). During the study period, Snake River discharge varied from ~ 14 to ~ 220 m^3/s (USGS, 2023b).

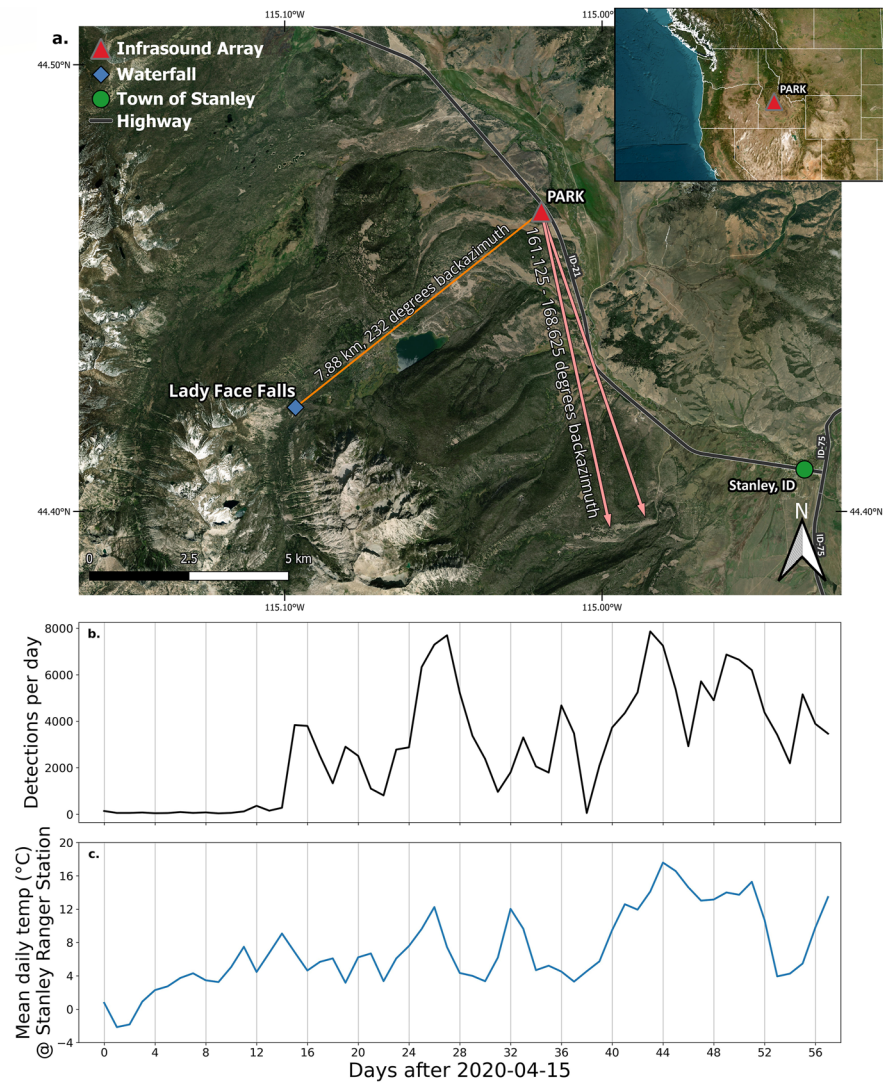


Figure 3. (a) Map of PARK infrasound array in relation to Lady Face Falls (LFF) and the azimuthal range of detections from Twin and Shoshone Falls. (b and c) Comparison of detections per day from LFF (227–237°) with temperature at Stanley Ranger Station (~15 km from LFF, and 100–950 m lower than the basin). Stanley Lake basin is primarily east, west, and north-aspect. The general trend shows infrasound detections increasing with warming temperatures.

Infrasound detections ranging from 161.125 to 168.625° backazimuth encompass Shoshone and Twin Falls (Figure 4a). Similar to LFF and other waterfall sources, infrasound from this range is quiet and continuous, although the long-term intermittency of detections is greater than that from LFF. The Twin Falls metropolitan area is also located within this range; however we find an anthropogenic source unlikely, as human temporal patterns are not observed.

The falls are detected at PARK some of the time when discharge exceeds $\sim 75 \text{ m}^3/\text{s}$, but are not detected when discharge drops below this threshold (Figures 4b and 4c). Follow-up recordings made approximately 200 m from Shoshone Falls indeed show that infrasound power is much higher at high flow ($92 \text{ m}^3/\text{s}$) than low flow ($10 \text{ m}^3/\text{s}$) (Figure S4 in Supporting Information S1), in accordance with our lack of detections in low-flow periods.

The intermittency of detections during high flow is unsurprising because infrasound arrivals at such a distance (i.e., just beyond the nearest shadow zone) depend on favorable stratospheric weather. Generally, infrasound either arrives directly, or requires atmospheric ducting (refractions dependent on stratospheric or thermospheric wind and temperature) to reach long distances. Acoustic shadow zones, where neither direct arrivals nor refractions of infrasound can reach, have long been recognized (Gutenberg, 1939). The nearest shadow zone often ranges from

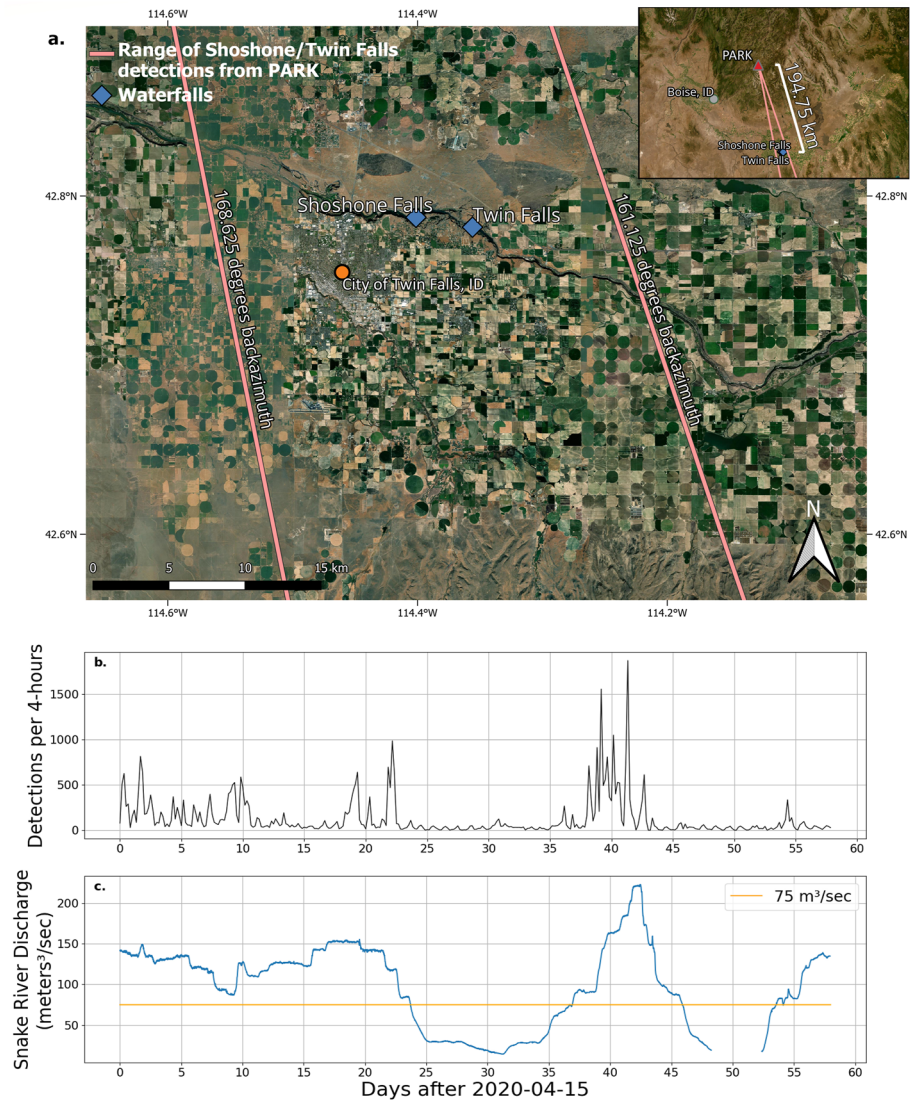


Figure 4. (a) Location Map of Shoshone and Twin Falls, with the bounds of infrasound detections represented with pink lines. (b) Number of infrasound detections per 4-hrs, from 162.125 to 168.625° backazimuth. Detections are intermittent, where we observe multi-day periods of both high and low detection values. (c) Snake River Discharge from USGS13090500, downstream of Shoshone and Twin Falls. The approximate threshold of 75 m³/s represents the minimum discharge where infrasound detections occur. Note that discharge measurements are unavailable from approximately day 48–52.

~70 to 150 km from the source (Farges et al., 2021); however, upper atmospheric temperature and wind velocity profiles change constantly, resulting in highly variable shadow zone extents (de Groot-Hedlin, 2017).

3.3. Thunderstorm Infrasound

Thunderstorm-generated infrasound is a prevalent sound source in the region, and many storms are recorded by the PARK array. We compared infrasound backazimuths during three periods of high storm activity with World Wide Lightning Location Network (WWLLN) data (Figure 5). The World Wide Lightning Location Network uses a network of very low frequency radio sensors to locate lightning strokes all over the globe (Lay et al., 2005). The comparison of infrasound and WWLLN data proved effective in identifying individual storms, where many densely-packed and slowly changing backazimuths match WWLLN location data. Although nearby storms are detected more often than far-away ones, they sometimes remain undetected. Thunderstorm characteristics, shadow zones (as discussed in Section 3.2), and atmospheric conditions may explain inconsistencies in PARK's ability to detect nearby thunder.

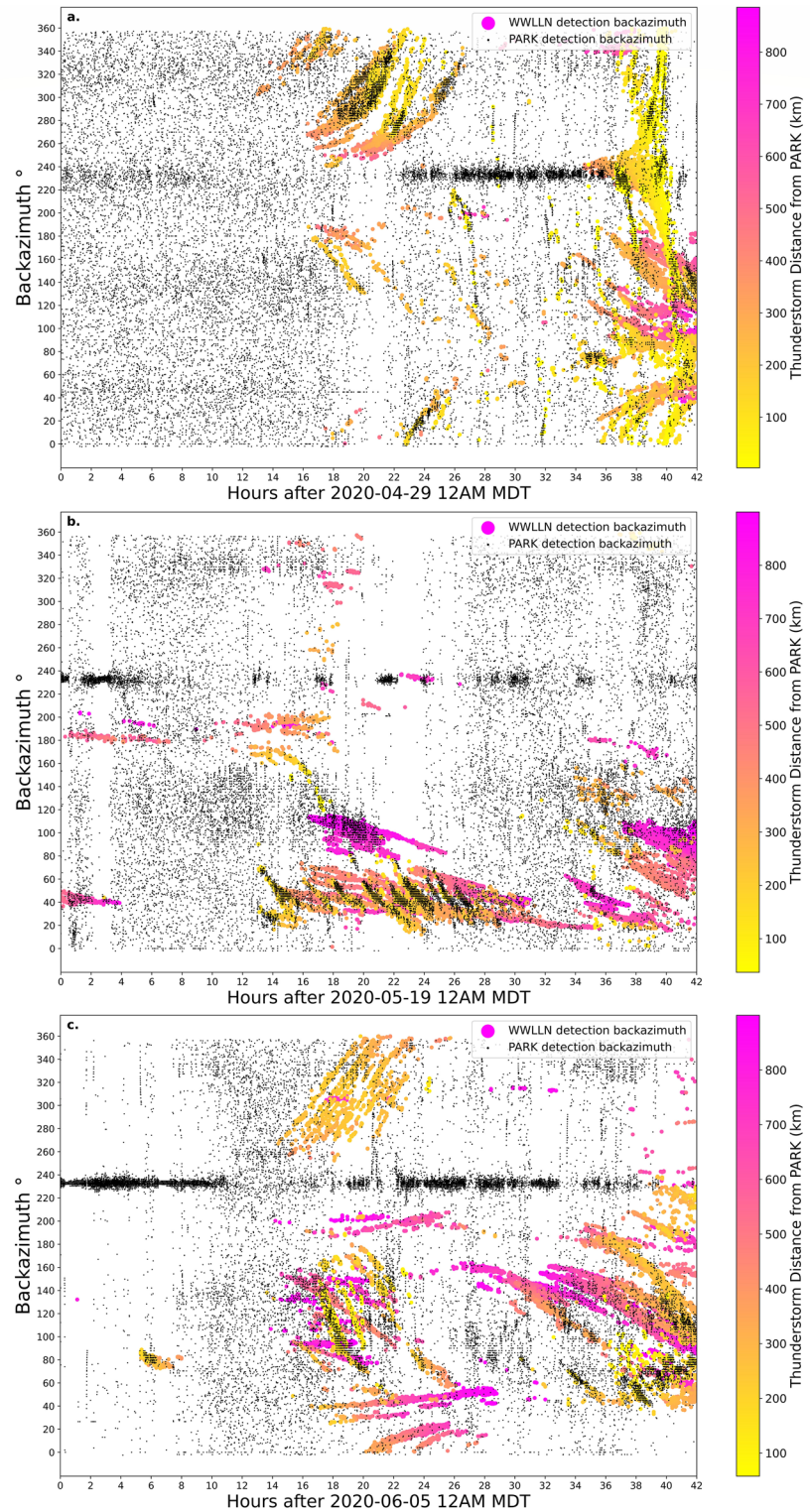


Figure 5. Comparison of infrasound detection backazimuth from PARK (black) and lightning detections from the World Wide Lightning Location Network (WWLLN) (colors). WWLLN colors represent the distance from a detection to the PARK array. Intermittent infrasound detections around $\sim 232^\circ$ radiate from Lady Face Falls. (a) Thunder from multiple lightning storms is detected throughout the day, although some storms lack infrasound detections. (b) Infrasound captured the repeated storms in the $20\text{--}80^\circ$ range, as well as a storm ~ 850 km away from hour 18 to 21. (c) Notice the lack of infrasound detections from fairly proximal storms in the $260\text{--}360^\circ$ range, where similarly located storms were detected in panel (a).

We observed much variation with time, backazimuth, and distance in PARK's ability to detect thunder infrasound, as is observed by Farges et al. (2021). For example, two storms on 29 April 2020 and 19 May 2020 share very similar characteristics; both storms appear from $\sim 260^\circ$ and dissipate at $\sim 360^\circ$, and their distances to PARK are similar (100–300 km). Despite these similarities, one storm is reasonably well-captured by infrasound data (Figure 5a), the other lacks detections altogether (Figure 5c). One well-tracked storm occurring on hour 22 at $\sim 280^\circ$ backazimuth that is (indicated by WWLLN) getting closer to PARK appears to lose detections altogether when it reaches a certain distance from the array (Figure 5a).

Thunderstorms moving in and out of shadow zones may contribute to this phenomenon. We also note azimuthal detection biases on all 3 days where thunder infrasound is only detected in certain, time-variable azimuth ranges despite the presence of thunderstorms at other ranges.

The furthest storm detected by infrasound was 800–900 km away from PARK, beginning hour 18 on 19 May 2020 in the $90\text{--}120^\circ$ range (Figure 5b). This particularly powerful storm was associated with 2.5 cm hail and 30 m/s winds and classified as “severe” (NOAA, 2020), and therefore may be more likely to be detected at long distances. Storm-generated infrasound detections at this distance is uncommon, but has been previously observed at distances exceeding 1,000 km (Bowman & Bedard, 1971).

3.4. Earthquake Infrasound

On 31 March 2020 a M6.5 earthquake occurred approximately 30 km northwest of Stanley, ID. Following this mainshock, the PARK infrasound array was established to monitor ensuing aftershocks. Here, we focus on primary earthquake infrasound from local earthquakes. Primary earthquake infrasound is the conversion of seismic to infrasonic waves at the array, propagating upwards. Near-zero slowness values are indicative of primary earthquake infrasound, as wave arrivals are nearly synchronous for all array elements due to the high seismic wave speeds (compared to infrasound). In the 5–20 Hz band of interest, near-zero slowness values associated with earthquakes are clearly visible, however below 5 Hz the presence of primary earthquake infrasound is absent (Figures S1–S3 in Supporting Information S1). We consider slowness values other than those associated with typical horizontal infrasound (centered around 3 s/km) and earthquakes to be likely wind noise.

Consecutive days with high concentrations of earthquake detections are observed near the beginning of the study period (Figure 2b). These higher concentrations are consistent with the rapid decay of aftershock occurrence soon after the mainshock (Liberty et al., 2020). After 2 May 2020 (day 17) near-zero slowness detections become more intermittent, and the occurrence of near-zero slowness detections correspond well with the 13 highest magnitude earthquakes ($\geq M3.2$) within 10 km of PARK (Figure 2b). For example, observations of slowness on 22 May 2020 reveal a significant number of near-zero slowness values immediately following a M3.8 earthquake (Figure 2j). Near-zero slowness values exist before the M3.8 because multiple earthquakes occurred in the hours beforehand, generating primary infrasound (USGS, 2023a). When looking at backazimuth values that coincide with the timing of this earthquake, we observe a potential source of secondary infrasound from $\sim 110^\circ$ where sporadic clusters of detections overpower the drone of LFF (Figure 2i). We interpret these increases in primary infrasound detections as swarms of small aftershocks (many being too small to be detected by a permanent seismic network) following a significant earthquake.

4. Conclusions

In order to better understand the capabilities of a large-N infrasound array (22 sensors over a 100 by 150 m area) we studied 58 days of data and identified diverse infrasonic sources. Signals from waterfalls, thunderstorms, and earthquakes were found, many of which are weak and may have been lost to background noise if only a 3-element array was used.

We recorded infrasound from a small waterfall 8 km from the PARK array, and found nearly continuous low-level radiation after mid-spring warming led to increased discharge from snowmelt. Intermittent, ducted infrasound was detected from two distant waterfalls (Twin and Shoshone Falls, at 195 km), during periods of high flow through the falls. Three periods of high thunderstorm activity were recorded and compared to WWLLN data, where thunder infrasound was identified at distances approaching 900 km. Aftershocks following the 2020 M6.5 Stanley, Idaho earthquake were associated with frequent infrasound over the following days with very low

horizontal slowness (typical of converted seismic waves), and uncovered low-magnitude earthquakes that may be unnoticeable to a permanent seismic network.

We demonstrate that, using a large-N array and standard beamforming method, infrasound scientists can identify a variety of phenomena that would otherwise be hidden in background noise and that the significant challenges of deploying and maintaining a large-N array can be mitigated by the use of small, low-power, cable-free instruments. We envision widespread application of large-N infrasound for identifying weaker signals than can normally be studied, both for traditional geophysical studies and in other disciplines. For example, we note that this strategy is useful for monitoring waterfalls at much longer ranges than would be possible ordinarily, with hydrological and geomorphological applications for monitoring stream morphology and discharge. Additionally, the improved sensitivity of large-N arrays to weak signals may facilitate monitoring atmospheric conditions using infrasound, either via ambient noise interferometry (Haney, 2009; Ortiz et al., 2021), passive-source (Johnson et al., 2012) or active-source (Averbuch et al., 2021). Finally, the logistical benefits of small, low-power instruments also apply to airborne infrasound (e.g., Garcia et al., 2021); potential applications of flying infrasound arrays include avoiding ground-level acoustic shadow zones and instead recording within acoustic waveguides, and performing aerial seismology on planets lacking a ground surface where seismometers can function.

Data Availability Statement

Infrasound data can be downloaded from IRIS-DMC via the data request form (network code XP, station code PARK) (Berti et al., 2020). World Wide Lightning Location Network data is available at nominal cost from the WWLLN website (Holzworth, 2023). Discharge data from the Snake River is available from the USGS, site No. 13090500 (USGS, 2023b). Earthquake event data is available from the USGS (USGS, 2023a). Beamforming of data used the Python package ObsPy (Krischer et al., 2015). Python code used in this paper to recreate Figures 2–5 and Figures S1–S5 in Supporting Information S1 can be found in a GitHub repository (Scamfer, 2023).

Acknowledgments

The authors thank T. Farges, and D. Bowman for their helpful discussion and insight. We acknowledge National Science Foundation awards EAR-2051670 and EAR-2029940. The authors wish to thank the WWLLN (<http://wwlln.net>), a collaboration among over 50 universities and institutions, for providing the lightning location data used in this paper.

References

- Anderson, J. F., Johnson, J. B., Arechiga, R. O., & Thomas, R. J. (2014). Mapping thunder sources by inverting acoustic and electromagnetic observations. *Journal of Geophysical Research: Atmospheres*, 119(23), 13287–13304. <https://doi.org/10.1002/2014JD021624>
- Anderson, J. F., Johnson, J. B., Bowman, D. C., & Ronan, T. J. (2018). The gem infrasound logger and custom-built instrumentation. *Seismological Research Letters*, 89(1), 153–164. <https://doi.org/10.1785/0220170067>
- Anderson, J. F., Johnson, J. B., Mikesell, T. D., & Liberty, L. M. (2023). Remotely imaging seismic ground shaking via large-N infrasound beamforming. *Communications Earth & Environment*, 4(1), 399. <https://doi.org/10.1038/s43247-023-01058-z>
- Arrowsmith, S. J., Hedlin, M. A. H., Stump, B., & Arrowsmith, M. D. (2008). Infrasonic signals from large mining explosions. *Bulletin of the Seismological Society of America*, 98(2), 768–777. <https://doi.org/10.1785/0120060241>
- Averbuch, G., Giannone, M. R., Arrowsmith, S., & Anderson, J. (2021). Evidence for short temporal atmospheric (tropospheric) variations observed by infrasonic signals. *Journal of the Acoustical Society of America*, 150(4), A178–A179. <https://doi.org/10.1121/10.0008045>
- Berti, C., Lee, L., Stachnik, J., & Mikesell, D. (2020). Aftershock deployment for Stanley, ID earthquake 2020 [Dataset]. International Federation of Digital Seismograph Networks. https://doi.org/10.7914/SN/XP_2020
- Bosa, A., Johnson, J., De Angelis, S., Lyons, J., Roca, A., Anderson, J., & Pineda, A. (2021). Tracking secondary lahar flow paths and characterizing pulses and surges using infrasound array networks at Volcán de Fuego, Guatemala. *Volcanica*, 4(2), 239–256. <https://doi.org/10.30909/vol.04.02.239256>
- Bowman, H. S., & Bedard, A. J. (1971). Observations of infrasound and subsonic disturbances related to severe weather. *Geophysical Journal of the Royal Astronomical Society*, 26(1–4), 215–242. <https://doi.org/10.1111/j.1365-246x.1971.tb03396.x>
- Capelli, A., Kapil, J. C., Reiweger, I., Or, D., & Schweizer, J. (2016). Speed and attenuation of acoustic waves in snow: Laboratory experiments and modeling with Biot's theory. *Cold Regions Science and Technology*, 125, 1–11. <https://doi.org/10.1016/j.coldregions.2016.01.004>
- Che, I.-Y., Park, J., Kim, I., Kim, T. S., & Lee, H.-I. (2014). Infrasound signals from the underground nuclear explosions of North Korea. *Geophysical Journal International*, 198(1), 495–503. <https://doi.org/10.1093/gji/ggu150>
- de Groot-Hedlin, C. D. (2017). Infrasound propagation in tropospheric ducts and acoustic shadow zones. *Journal of the Acoustical Society of America*, 142(4), 1816–1827. <https://doi.org/10.1121/1.5005889>
- Evers, L. G., & Haak, H. W. (2005). The detectability of infrasound in The Netherlands from the Italian volcano Mt. Etna. *Journal of Atmospheric and Solar-Terrestrial Physics*, 67(3), 259–268. <https://doi.org/10.1016/j.jastp.2004.09.002>
- Farges, T., Hupe, P., Le Pichon, A., Ceranna, L., Listowski, C., & Diawara, A. (2021). Infrasound thunder detections across 15 years over Ivory Coast: Localization, propagation, and link with the stratospheric semi-annual oscillation. *Atmosphere*, 12(9), 1188. <https://doi.org/10.3390/atmos12091188>
- Fee, D., & Matoza, R. S. (2013). An overview of volcano infrasound: From Hawaiian to plinian, local to global. *Journal of Volcanology and Geothermal Research*, 249, 123–139. <https://doi.org/10.1016/j.jvolgeores.2012.09.002>
- Garcia, R. F., Martire, L., Chaigneau, Y., Cadu, A., Mimoun, D., Bassas Portus, M., et al. (2021). An active source seismo-acoustic experiment using tethered balloons to validate instrument concepts and modelling tools for atmospheric seismology. *Geophysical Journal International*, 225(1), 186–199. <https://doi.org/10.1093/gji/ggaa589>
- Gutenberg, B. (1939). The velocity of sound waves and the temperature in the stratosphere in southern California. *Bulletin of the American Meteorological Society*, 20(5), 192–201. <https://doi.org/10.1175/1520-0477-20.5.192>

- Haney, M. M. (2009). Infrasonic ambient noise interferometry from correlations of microbaroms. *Geophysical Research Letters*, 36(19), L19808. <https://doi.org/10.1029/2009GL040179>
- Holzworth, R. (2023). WWLLN: World Wide Lightning Location Network [Dataset]. WWLLN. <http://wwlln.net>
- Johnson, J. B., Anderson, J., Marcillo, O., & Arrowsmith, S. (2012). Probing local wind and temperature structure using infrasound from Volcan Villarrica (Chile). *Journal of Geophysical Research*, 117(D17), D17107. <https://doi.org/10.1029/2012jd017694>
- Johnson, J. B., Anderson, J. F., Marshall, H. P., Havens, S., & Watson, L. M. (2021). Snow avalanche detection and source constraints made using a networked array of infrasound sensors. *Journal of Geophysical Research: Earth Surface*, 126(3), e2020JF005741. <https://doi.org/10.1029/2020jf005741>
- Johnson, J. B., Lees, J. M., & Yepes, H. (2006). Volcanic eruptions, lightning, and a waterfall: Differentiating the menagerie of infrasound in the Ecuadorian jungle. *Geophysical Research Letters*, 33(6), L06308. <https://doi.org/10.1029/2005gl025515>
- Johnson, J. B., Mikesell, T. D., Anderson, J. F., & Liberty, L. M. (2020). Mapping the sources of proximal earthquake infrasound. *Geophysical Research Letters*, 47(23), e2020GL091421. <https://doi.org/10.1029/2020gl091421>
- Johnson, J. B., & Ripepe, M. (2011). Volcano infrasound: A review. *Journal of Volcanology and Geothermal Research*, 206(3–4), 61–69. <https://doi.org/10.1016/j.jvolgeores.2011.06.006>
- Kogelnig, A., Hübl, J., Surinach, E., Vilajosana, I., & McArdell, B. W. (2014). Infrasound produced by debris flow: Propagation and frequency content evolution. *Natural Hazards*, 70(3), 1713–1733. <https://doi.org/10.1007/s11069-011-9741-8>
- Krischer, L., Megies, T., Barsch, R., Beyreuther, M., Lecocq, T., Caudron, C., & Wassermann, J. (2015). ObsPy: A bridge for seismology into the scientific Python ecosystem [Software]. *Computational Science & Discovery*, 8(1), 014003. <https://doi.org/10.1088/1749-4699/8/1/014003>
- Lay, E. H., Rodger, C. J., Holzworth, R. H., & Dowden, R. L. (2005). Introduction to the World Wide Lightning Location Network (WWLLN). *Geophysical Research Abstracts*, 7, 02875.
- Liberty, L. M., Lifton, Z. M., & Dylan Mikesell, T. (2020). The 31 March 2020 MW 6.5 Stanley, Idaho, earthquake: Seismotectonics and preliminary aftershock analysis. *Seismological Research Letters*, 92(2A), 663–678. <https://doi.org/10.1785/0220200319>
- Mutschlechner, J. P., & Whitaker, R. W. (2005). Infrasound from earthquakes. *Journal of Geophysical Research*, 110(D1), D01108. <https://doi.org/10.1029/2004jd005067>
- Nishida, K., Kawakatsu, H., Fukao, Y., & Obara, K. (2008). Background Love and Rayleigh waves simultaneously generated at the Pacific Ocean floors. *Geophysical Research Letters*, 35(16), L16307. <https://doi.org/10.1029/2008GL034753>
- NOAA. (2020). *Storm events database*. NOAA.gov. Retrieved from <https://www.ncdc.noaa.gov/stormevents/eventdetails.jsp?id=882894>
- Ortiz, H. D., Matoza, R. S., Johnson, J. B., Hernandez, S., Anzieta, J. C., & Ruiz, M. C. (2021). Autocorrelation infrasound interferometry. *Journal of Geophysical Research: Solid Earth*, 126(4), e2020JB020513. <https://doi.org/10.1029/2020jb020513>
- Ronan, T. J., Lees, J. M., Mikesell, T. D., Anderson, J. F., & Johnson, J. B. (2017). Acoustic and seismic fields of hydraulic jumps at varying Froude numbers. *Geophysical Research Letters*, 44(19), 9734–9741. <https://doi.org/10.1002/2017gl074511>
- Sanderson, R. W., Matoza, R. S., Haymon, R. M., & Steidl, J. H. (2021). A pilot experiment on infrasonic lahar detection at Mount Adams, cascades: Ambient infrasound and wind-noise characterization at a quiescent stratovolcano. *Seismological Research Letters*, 92(5), 3065–3086. <https://doi.org/10.1785/0220200361>
- Scamfer, L. T. (2023). LargeN_Infrasound_Paper [Software]. GitHub Repository. https://github.com/loganscamfer/LargeN_Infrasound_Paper
- Tatum, T. A., Anderson, J. F., & Ronan, T. J. (2023). Whitewater sound dependence on discharge and wave configuration at an adjustable wave feature. *Water Resources Research*, 59(8), e2023WR034554. <https://doi.org/10.1029/2023wr034554>
- Ulivieri, G., Marchetti, E., Ripepe, M., Chiambretti, I., De Rosa, G., & Segor, V. (2011). Monitoring snow avalanches in Northwestern Italian Alps using an infrasound array. *Cold Regions Science and Technology*, 69(2–3), 177–183. <https://doi.org/10.1016/j.coldregions.2011.09.006>
- U.S. Geological Survey. (2023a). Earthquake Catalog [Dataset]. USGS. Retrieved from <https://earthquake.usgs.gov/earthquakes/search/>
- U.S. Geological Survey. (2023b). Snake River NR Twin Falls ID - 13090500 [Dataset]. USGS. Retrieved from <https://waterdata.usgs.gov/monitoring-location/13090500/#parameterCode=00060&startDT=2020-04-15&endDT=2020-06-11>